

ARTICLE

Experimental study of moment redistribution in continuous concrete beams prestressed with unbonded tendons

Tarja Nakari  | Joonas Tulonen  | Olli Asp  | Ulla Kytölä  | Anssi Laaksonen 

Faculty of Built Environment—Concrete and Bridge Structures, Tampere University, Tampere, Finland

Correspondence

Tarja Nakari, Faculty of Built Environment—Concrete and Bridge Structures, Tampere University, Tampere, Finland.

Email: tarja.nakari@tuni.fi

Funding information

Finnish concrete industry

Abstract

The moment redistribution in a continuous prestressed concrete beam occurs as a result of a change in the rigidity of a beam and formation of plastic hinges when approaching the failure. Rotation capacity is required to allow for moment redistribution. Four continuous two-span concrete beams prestressed with unbonded tendons were built and loaded up to failure at the laboratory of Civil Engineering in Tampere University. The test beams had different reinforcement ratios in the support area when the degree of prestressing and amount of tension reinforcement in the midspans were kept constant. All test beams were loaded by bending, but one test beam had torsion load in addition to bending. The degree of bending moment redistribution was defined by using nonlinear analysis and equations from the European standard and ACI318, as well as the test results. Moment redistribution clearly occurred on all test beams, and the beams had a high level of deformability.

KEYWORDS

moment redistribution, post-tensioned concrete beam, prestressed concrete, unbonded tendon

1 | INTRODUCTION AND RESEARCH SIGNIFICANCE

In prestressed concrete structures, the stress of prestressing steel $\sigma_{p,ULS}$ is used to determine the flexural capacity. The dimensioning principles differ between bonded and unbonded prestressed concrete members. In a bonded post-tensioned concrete (BPC) beam, the flexural capacity, stresses and strains can be defined by using the principles of strain compatibility. In an unbonded post-tensioned concrete (UPC) beam, the determination of the

stress increment of the prestressing steel $\Delta\sigma_{p,ULS}$ at the ultimate limit state is more complicated because there is no bond between the tendon and surrounding concrete. The unbonded tendon can slide relative to the adjacent concrete. Thus, the principles of strain compatibility are no longer fulfilled.

The unbonded tendon is only connected to the concrete beam at both ends by anchors. The deformations of the UPC beam under loading have a substantial effect on the elongation and stress increase of the unbonded strands. Several researchers have proposed empirical

This is an open access article under the terms of the [Creative Commons Attribution](https://creativecommons.org/licenses/by/4.0/) License, which permits use, distribution and reproduction in any medium, provided the original work is properly cited.

© 2024 The Authors. *Structural Concrete* published by John Wiley & Sons Ltd on behalf of International Federation for Structural Concrete.

equations for design purposes to determinate the stress increase of unbonded tendon at ultimate capacity.^{1–6} The latest studies of the behavior of continuous structures post-tensioned with unbonded tendons have revealed that the failure mechanisms of the simple-span system and continuous system are essentially different. For example, the dimensions of the beam, reinforcement ratios at the support and in the span, prestressing force, loading pattern, cracking of tension surface and formation of plastic hinges affect the deformation of the continuous beam. Moment redistribution in continuous structures has also been estimated in recent experimental studies.^{7,8} Even so, there are quite a few studies that have conducted a load test of continuous UPC structures in laboratory conditions.^{7–11}

The main objective of this research was to get more information about the behavior of a continuous concrete beam post-tensioned with unbonded tendons when approaching failure using load tests in laboratory conditions. This study aimed to find out the degree of moment redistribution of the continuous UPC structures under external loading. The test beams had different reinforcement ratios in the centre support area. They were loaded by bending, but one test beam had torsion load in addition to bending. The effect of torsion loading on moment redistribution of the UPC structure was examined at a general level, with further, more detailed examining of the torsion being withheld in this study.

Recently, more detailed numerical simulation of the behavior of UPC members was presented in several research papers.^{12,13} These complex simulations were usually based on nonlinear finite element analyses. Comparison calculations of test results have been made by using a simplified non-linear analysis in this article as well.¹⁴

Lou et al. proposed a modification to the ACI318 equation of calculating the allowable moment redistribution in continuous prestressed structures.¹⁵ The effect of the relative rigidity of a continuous UPC member was proposed in their article. It was applied by using the parameter ω_{q1}/ω_{q2} , where ω_{q1} and ω_{q2} were mechanical reinforcement ratios at critical sections like centre support and mid-span. The proposed equation is used to determine the moment redistribution of the test beams in this study.

Moment redistribution has been handled rather briefly in the European standard EN 1992-1-1.¹⁶ The equations for the ratio of the redistributed moment to elastic bending moment does not take into account the effect of bonded or unbonded prestressing. This study has examined how well these models presented above work for estimating the degree of moment redistribution of a continuous UPC structure.

2 | EXPERIMENTAL PROGRAMME

Four continuous two-span concrete beams prestressed with unbonded tendons were built and loaded up to failure at the laboratory of Civil Engineering in Tampere University. There were two equal 10 m spans in the test beams (B1-B4). All beams had the same T-shaped cross-section with 150 mm wide flanges. The width of the web was 700 mm, with a total beam width of 1000 mm. The total height of the beam was 500 mm and the flange thickness was 100 mm. All tested beams had the same amount of unbonded tendons, and the degree of prestressing was kept constant. By contrast, the amount of reinforcement bars at the section of centre support varied between the tested beams. The test beams were close to half-scale (60%) when compared to the dimensions of a typical floor structure of a car park.

2.1 | Test beams' design and fabrication

All test beams were post-tensioned with eight unbonded mono-strands with similar tendon geometry. The symmetrical tendon profile consisted of parabolic segments. The geometry of one half of the tendon profile is shown in Figure 1.

All test beams had the same amount of non-prestressed reinforcement in both mid-spans and ends of the beam. The beams differed in terms of support reinforcement. In beam B1, the amount of tension reinforcement steel bars satisfied the requirement of the minimum area of bonded reinforcement according to European standard EN 1992-1-1.¹⁶ In beam B2, the tension reinforcement was doubled at the section of the centre support. Beam B3 had the same reinforcement as beam B2, but six compression reinforcement bars were added to the compression zone in the centre support. The last test beam B4 had the same tension reinforcement arrangement as beam B2, but it was loaded with torsional loading in addition to bending. Other test beams were loaded by bending only.

The shear reinforcement of all test beams consisted of U-shaped stirrups in the beam web and two opposite U-shaped stirrups in the flange of the beam. The spacing of the stirrups was constant (100 mm) except at the ends of beam B4, where the spacing was shorter (75 mm). A relatively high shear reinforcement ratio was used in order to avoid shear failure during the load tests. Additional stirrups for the local crushing and transverse tension forces were used in the anchoring zones of the unbonded tendons. The reinforcement arrangement of the beams can be seen in Figure 2. The information of the reinforcement has been summarized in Table 1.

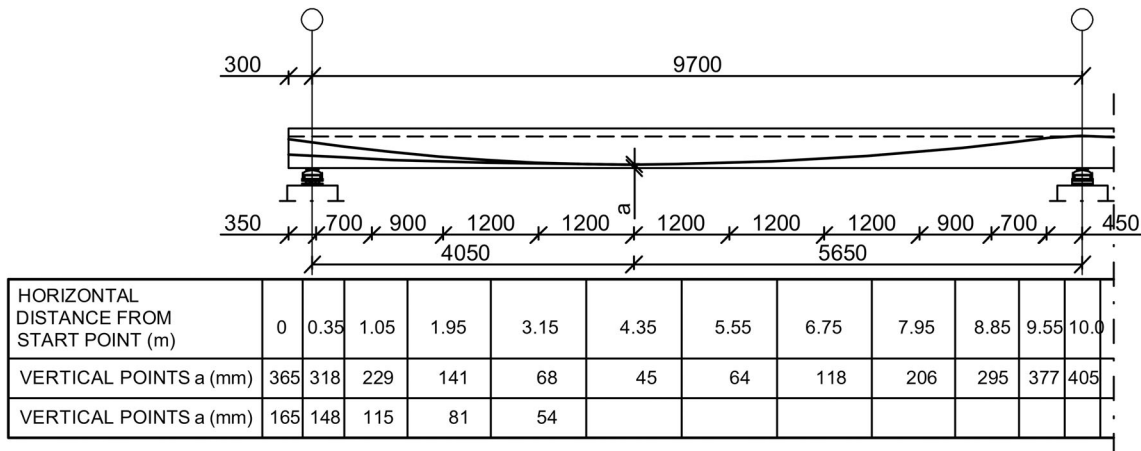


FIGURE 1 Tendon geometry.

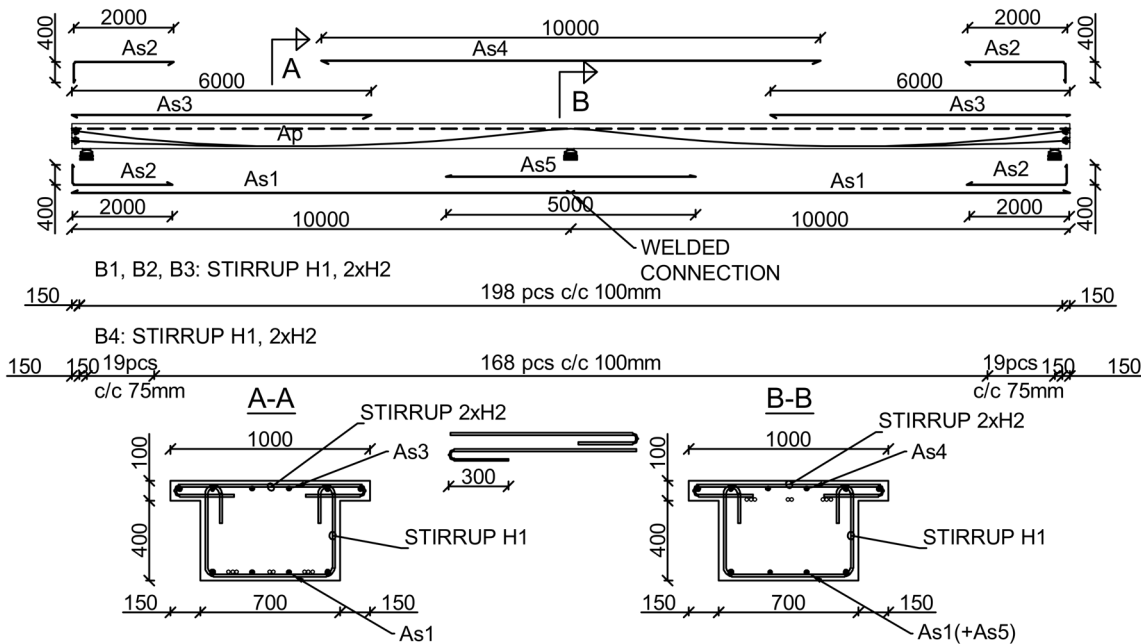


FIGURE 2 Reinforcement arrangement of test beams.

2.2 | Material properties of test beams

The designed concrete class was C30/37 according to European standard EN 1992-1-1.¹⁶ During the casting, 12 pcs of test cylinders ($d = 150$ mm and $h = 300$ mm) were cast from concrete batches of each test beam. These were used to monitor the development of concrete compression strength. Moist curing under plastic foil took place around 14 days. The average concrete cylinder strength varied between 38 and 43 MPa. The results are shown in Table 2.

The unbonded post-tensioned tendon consisted of a seven-wire strand ($A_p = 149.55$ mm²) covered with grease and a plastic cover. The characteristic 0.1% proof-stress of the prestressing steel (Y1860S7) was $f_{p0.1k} = 1693$ MPa, the

maximum characteristic tensile strength $f_{pk} = 1883$ MPa, the modulus of elasticity $E_p = 201.7$ GPa and the elongation at maximum force was 4.8% according to the test certificate of used strands.¹⁷ The effective prestress used in the load tests varied slightly between test beams. The relatively low value of the prestressing (around 1000 MPa) simulated the long-term stress losses that occur in an actual structure.

The non-prestressing reinforcement was ordinary mild steel bars (B500B) with yield strength $f_y = 500$ MPa, maximum tensile strength $R_m = 550$ MPa and modulus of elasticity $E_s = 200$ GPa. The percentage total elongation at maximum force $\epsilon_{uk} = 5\%$ was used in comparison calculations. The reinforcement arrangement of the test beams is presented in Table 1 and Figure 2.

TABLE 1 Reinforcement of test beams.

Test beam	A_{s1} (mm ²)	A_{s2} (mm ²)	A_{s3} (mm ²)	A_{s4} (mm ²)	A_{s5} (mm ²)	Stirrups H1 (#12)	Flange stirrups H2 (#12, 2-par bundles)
B1	628 (2#16 + 2#12)	452 (4#12)	678 (6#12)	678 (6#12)	0	198 pcs c/c 100 mm	198 pcs c/c 100 mm
B2	628 (2#16 + 2#12)	452 (4#12)	678 (6#12)	1357 (12#12)	0	198 pcs c/c 100 mm	198 pcs c/c 100 mm
B3	628 (2#16 + 2#12)	452 (4#12)	678 (6#12)	1357 (12#12)	678 (6#12)	198 pcs c/c 100 mm	198 pcs c/c 100 mm
B4	628 (2#16 + 2#12)	452 (4#12)	678 (6#12)	1357 (12#12)	0	208 pcs c/c 75 mm/100 mm	198 pcs c/c 100 mm

2.3 | Instrumentation

The strains on the surfaces of the test beams and in the reinforcing bars were measured with two different methods. The strain gauges (SGB) were attached to the longitudinal top and bottom reinforcing bars as well as to the stirrups near the centre support. The strains in the reinforcement bars during prestressing and the load test were recorded with this measurement instrumentation. The locations of the strain gauges are shown in Figure 3.

The displacement gauges (LVDT) were used to measure the strains on the different surfaces of the test beams, a rotation of the support area and deflections of the beam. These were installed mainly after prestressing, so only deformations during the load test were recorded by these gauges. Two displacement gauges were used in the prestressing phase to measure the deflection of both spans. The more precise locations of those sensors, that are evaluated later in this study, are presented in Figure 3. The deformation data of both gauges were saved 10 times per second.

In addition, the force in the unbonded strands was measured with force sensors from both anchors of two tendons in each test beam. The tendon force was measured both during the prestressing of the tendons and during the load test.

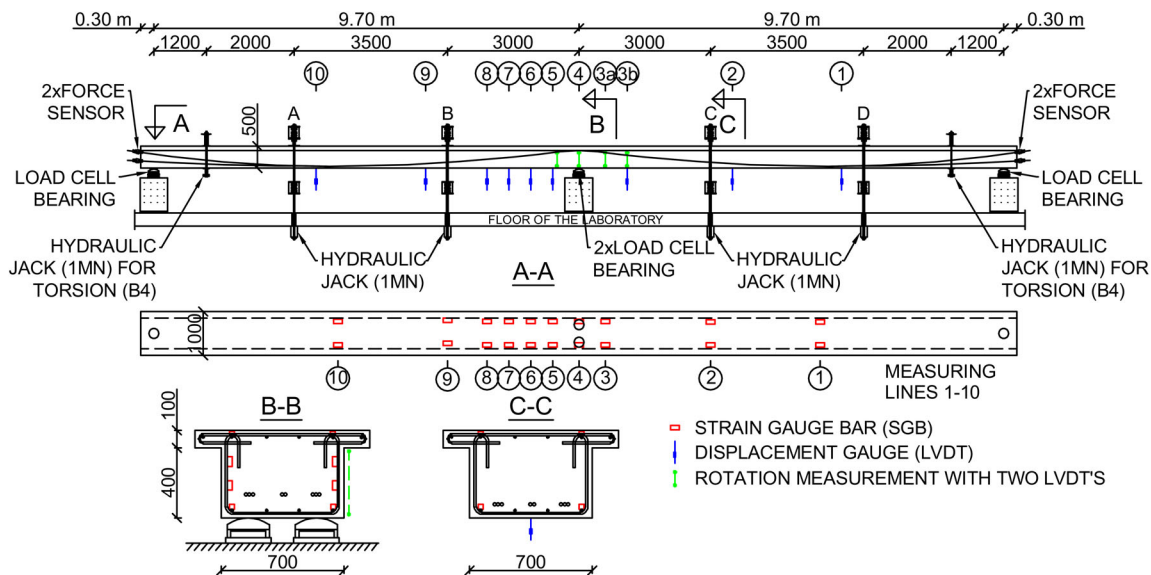
2.4 | Test setup in the laboratory

At the age of around 100 days, the beam was lifted onto the supports. At this point there was an additional support in the middle of both spans. The tendons were prestressed at the final load testing position between 2 and 7 days after installation on the supports. After that, the remaining measuring and loading arrangements were installed. About a week after prestressing the load test was performed. The ages of the beam at different phases can be seen from Table 2.

The load was applied with two point loads on each span. The location of the point loads from the support was approximately one third of the span length. The test beam B4 was loaded by torsion load in addition to the bending loads. The point loads were applied by four displacement-controlled hydraulic jacks with a capacity of 1000 kN. Steel frames for the test arrangement transmitted the load from the hydraulic jacks to the beam, see Figure 4. The loads in load frames A and D were around 60% to 70% of the loads in load frames B and C, which simulated a uniform load. The load values of each hydraulic jacks at different load steps were recorded by the measurement program so that the same values were able to be used later in the nonlinear analysis. In this

TABLE 2 Test results from loading tests of compression test cylinders and the age of the concrete at different phases.

Test beam	Age of concrete at post-tensioning (days)	Average concrete compression strength at time of post-tensioning (MPa)	SD (MPa)	Age of concrete at load test (days)	Average concrete compression strength at time of loading (MPa)	SD (MPa)
B1	104	39.17	0.56	114	38.92	1.31
B2	118	43.49	0.92	123	43.32	1.05
B3	103	37.99	0.97	105	37.64	0.40
B4	117	37.92	0.63	124	38.86	0.64


FIGURE 3 Test setup and instrumentation.

load arrangement, the deformations of the span are more localized than when the uniform load is used. However, the point loads were used in order to simplify the load arrangements.

Plain bearings were located under both ends of the test beams (shown in Figure 5). These allowed longitudinal displacement and rotations around all axes. On the centre support, there were two bearings side by side which allowed rotation, but not translational displacements, of the beam. All bearings had force sensors for measuring the support reaction during different phases of the test, for example prestressing and loading. At the loading of the test beam B4, the hydraulic jacks for torsion were located 1.2 m from both end supports of the beam.

A load program was prepared for each test beam. The external loads consisted of a permanent load which represented the self-weight of a continuous floor structure of a typical car park, and an imposed live load of 5 kN/m^2 according to European standard EN 1991-1-1, that is, the traffic area category G.¹⁸ Both of these loads

were converted into the scale of the load test (60% of the actual structure). The uniform loads were changed into two point loads which represented the uniform load as well as possible.

The program included four load steps, after which the load was removed. The first two load levels represented long-term SLS loading according to European standard EN 1990, where live load was multiplied with the factor $\psi_2 = 0.3$.¹⁹ The second two steps represented frequent SLS loading with the factor $\psi_1 = 0.5$ and the fifth load step represented characteristic SLS loading with the factor $\psi = 1.0$.¹⁹ After that step, the loads in the hydraulic jacks were increased until the maximum deflection capability of the test setup occurred. The load steps of the hydraulic jack varied from 10 to 60 kN, and the loading rate was around 20 kN/min per jack. The torsion load 80 kNm was first imposed to beam B4 at the level of frequent SLS loading, and it was raised to the level 120 kNm during the load test. After each load step, visible cracks were highlighted with a marker pen and the crack width of a few selected cracks was measured with a



FIGURE 4 Test setup and instrumentation of test beam B4.

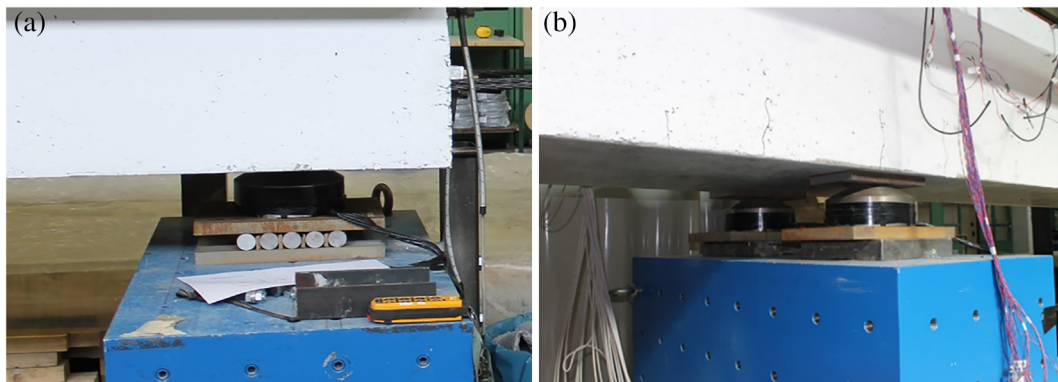


FIGURE 5 Plain bearings on the end (a) and centre (b) support of test beam B1.

crack measuring loupe. For safety reasons, this was continued somewhat below the level where the capacity of the test beam determined according to European standards was reached. The final crack patterns were highlighted after failure and after the loads were removed.

3 | METHODS TO CALCULATE DEGREE OF BENDING MOMENT REDISTRIBUTION IN TEST BEAMS

3.1 | Nonlinear analysis

A refined calculation was performed by using a nonlinear analysis.¹⁴ First, a moment-curvature relationship for a reinforced concrete cross-section under different axial

forces was determined. These were defined for all differently reinforced parts of the test beams. An amount of unbonded prestressing steel was not directly included in the calculation of the moment-curvature relationships. The effective prestress (axial) force and its eccentricity have been added later in the FE analysis by bar elements.

In the determination of moment-curvature relationships for different cross-sections, the compressive force is assumed to act on the centre of gravity of the cross-section. The tension strength of concrete has not been considered in the determination of the cross-sectional balance. The effect of concrete tension stiffening and confinement near the centre support has been neglected in this analysis for the sake of simplicity. The value for the ultimate compression strain of 3.5‰ is adopted from EN 1992-1-1.¹⁶

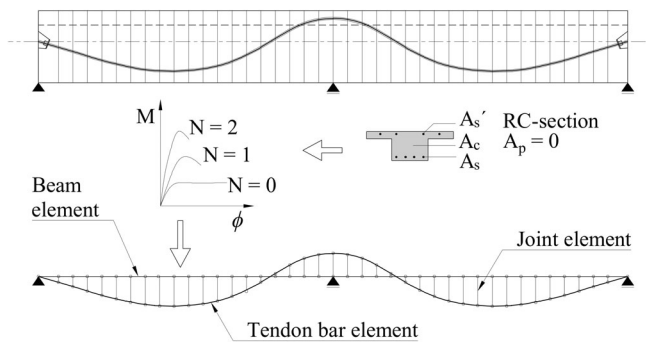


FIGURE 6 Finite element model of the beam and tendon.¹⁴

The nonlinear finite element analysis program LUSAS was used.²⁰ The test beams were modeled by using 3D beam elements. The moment-curvature relationships of a differently reinforced cross-section with eight levels of axial force were derived and entered as a user-defined material model in the FE program, seen in Figure 6.¹⁴ The intermediate values were defined by linear interpolation.

The tendon geometry was modeled as a resultant of a group of eight mono-strands.

The bar elements were modeled separately from the gravity line of the concrete beam conforming to the actual geometry of the tendon resultant. This way the eccentricity of the tendon was included in the model. The bar element division was such that the nodes were located on the same vertical line as the node in the beam. These nodes were connected by a 3D joint element that connects two nodes by three springs in the local x-, y-, and z-directions and does not have rotational stiffness. In the direction of the beam axis, the elastic stiffness of the spring is set high, but in the other two directions the movement is permitted. The bar elements were rigidly connected to the beam elements only at both ends of the whole beam structure. The bending moment capacity obtained from the model includes the moments from external loads (dead and live loads) as well as the secondary moment. The secondary moment develops when loading the structure in relation to the stiffness of the cross-section.¹⁴

The nonlinear analysis includes the change in arc length but not the dilatation of the beam as the deflection of the beam increases. This also effects the additional strain $\Delta\epsilon_p$ of the prestressing steel. For this reason, a temperature increase ($\Delta T \approx 50^\circ\text{C} - 70^\circ\text{C}$) has been given to the beam elements in the nonlinear FE analysis at high load levels to simulate this expansion of the length of the test beam. The temperature increase used in the analysis has been chosen so that the deflection of the FE-model corresponded well with the results from the load tests. The influence of the temperature increase on the results was around 5%.

Moment redistribution depends primarily on the relative rigidity between critical cross-sections of the beam, centre support area and mid-span. The reinforcement ratios of these cross-sections affect the crack formation and yielding of the reinforcing bars, and thus the relative rigidity of the section under increasing external load.

In the comparison calculations, percentage bending moment redistribution in failure has been determined by using the Equation (1):

$$\delta(\%) = \frac{M_u^e - M_u^c}{M_u^e} * 100 \quad (1)$$

where M_u^e is the calculated moment according to elastic theory and M_u^c is the equivalent moment capacity calculated by using the nonlinear analysis.

When examining the test results, the M_u^c was determined from the test results (from loads and supports reactions) at the different load levels as is presented in chapter 5.2. Then the moment redistribution has calculated by using the Equation (1).

The results are collected in Table 5, presented in chapter 5.3.

The nonlinear stress-strain relation for the concrete under short-term uniaxial loading according to the European standard EN 1992-1-1 has been chosen to be used in comparison calculations.¹⁶ The expression is:

$$\frac{\sigma_c}{f_{cm}} = \frac{k\eta - \eta^2}{1 + (k-2)\eta} \quad (2)$$

where $\eta = \epsilon_c / \epsilon_{c1}$ ϵ_{c1} is the strain at peak stress, according to EN 1992-1-1 table 3.1. $k = 1.05 E_{cm} \times |\epsilon_{c1}| / f_{cm}$ (f_{cm} and E_{cm} according to table 3.1).

Expression (1) is valid for $0 < |\epsilon_c| < |\epsilon_{cu}|$ where ϵ_{cu} is the nominal ultimate strain. The value for the ultimate compression strain ϵ_{cu} is -3.5% .

A bilinear material model without strain hardening presented in EN 1992-1-1 was adopted for the reinforcing steel B500B used in test beams for sake of simplicity.¹⁶ The stress-strain curve for steel was assumed to be identical in tension and compression. The material properties of reinforcing steel are presented in chapter 2.2. The material properties of prestressing steel used in the nonlinear FE analysis were adopted from the test certificate of used strands.¹⁷ They are presented in the previous chapter.

3.2 | Calculation by using the proposed new formula of ACI318

In prestressed concrete structure, bonded tendons have normally yielded at failure. Unlike bonded tendons, unbonded strands are usually in their elastic range when

approaching the ultimate. Therefore, UPC members have different rigidity characteristics than bonded post-tensioned concrete members. That will lead to different behavior on bending moment redistribution. For that reason, Lou et al. included the effect of unbonded tendons to the relative rigidity of the UPC members in their proposed modification of the ACI318 equation of calculating the allowable moment redistribution in continuous prestressed concrete structures.¹⁵

They presented the tensile reinforcement index ω_q for a UPC member. The expression is:

$$\omega_q = \frac{A_p \sigma_{P0} + A_s f_y}{b d_p f_{ck}} \quad (3)$$

where b is cross-sectional width, d_p is depth from the extreme compression fiber to the centre of the prestressing steel, A_p and A_s are prestressing and reinforcing steel areas, f_y is yield strength of reinforcing steel, f_{ck} is concrete cylinder compressive strength and σ_{P0} is initial prestress.

The relative rigidity of a continuous UPC member has been expressed by the parameter ω_{q1}/ω_{q2} , where the parameter ω_{q1} is the reinforcement index of the mid-span in a two-span beam and the parameter ω_{q2} is the reinforcement index of centre support, respectively.

In their article, the modification of the ACI318 empirical equation has been proposed by including a coefficient λ_p related to ω_{q1}/ω_{q2} ; that is:

$$\delta(\%) = \lambda_p (1000 \varepsilon_t) \quad (4)$$

$$\lambda_p = 1.0 + 4.7 \ln \left(\frac{\omega_{q1}}{\omega_{q2}} \right) - 5.0 \ln^2 \left(\frac{\omega_{q1}}{\omega_{q2}} \right) + 3.6 \ln^3 \left(\frac{\omega_{q1}}{\omega_{q2}} \right) \quad (5)$$

where ε_t is extreme tension steel strain at ultimate, suggested to be >0.0075 , where parameter ω_{q1}/ω_{q2} is expressed earlier.^{15,21}

In this article, these proposed formulas have been used to determine the degree of moment redistribution of the test beams and compared with other calculation methods and test results.

3.3 | Calculation by using Eurocode equations

Bending moment redistribution is briefly discussed in European standard EN 1992-1-1 in chapter 5.5.¹⁶ Formulas are presented for the ratio of the redistributed

moment to the elastic bending moment in continuous beams and slabs at plastic phase with certain limitations. The members should predominantly be subject to flexure and they should have the ratio of the lengths of adjacent spans in the range of 0.5 to 2. The equations are:

$$\delta \geq k_1 + \frac{k_2 x_u}{d} \text{ for } f_{ck} \leq 50 \text{ MPa} \quad (6)$$

$$\delta \geq k_3 + \frac{k_4 x_u}{d} \text{ for } f_{ck} > 50 \text{ MPa} \quad (7)$$

$\geq k_5$ where Class B or Class C reinforcement is used and $\geq k_6$ where Class A reinforcement is used. where x_u is the depth of the neutral axis at the ultimate limit state after redistribution and d is the effective depth of the section.

The values for parameters k may be found in the National Annex. The recommended values are the following: $k_1 = 0.44$, $k_2 = 1.25(0.6 + 0.0014/\varepsilon_{cu2})$, $k_3 = 0.54$, $k_4 = 1.25(0.6 + 0.0014/\varepsilon_{cu2})$, $k_5 = 0.7$ and $k_6 = 0.8$. ε_{cu2} is the ultimate strain according to table 3.1 in the European standard EN 1992-1-1.¹⁶

Bending moment redistribution of continuous post-tensioned concrete members is not directly included in the above equations.

4 | OBSERVATIONS FROM LOAD TESTS

4.1 | Crack formation and deflection of test beams

The test beams were visually observed after they were lifted onto the supports. A thin crack was detected over the centre support at the top surface of the cross-section in beams B1, B3, and B4. This had been formed during curing of concrete and lifting and placing the beam onto the supports. The crack was closed while the beam was prestressed. In the same test beams, a few cracks were also detected at the bottom of the cross-section over the centre support after prestressing (shown in Figure 5). These cracks closed when the external load was increased during the load test. In beam B2, any visible cracks were not observed before the load test.

During loading, the first individual cracks occurred on the top surface of the cross-section over the centre support. When the external load was slightly increased, primary cracks also formed on the bottom surface of the beam under the outermost loading frames. These appeared at a load level of 27% to 34% of the failure load. After the load was removed, the cracks closed. The pattern of the cracks was stable.

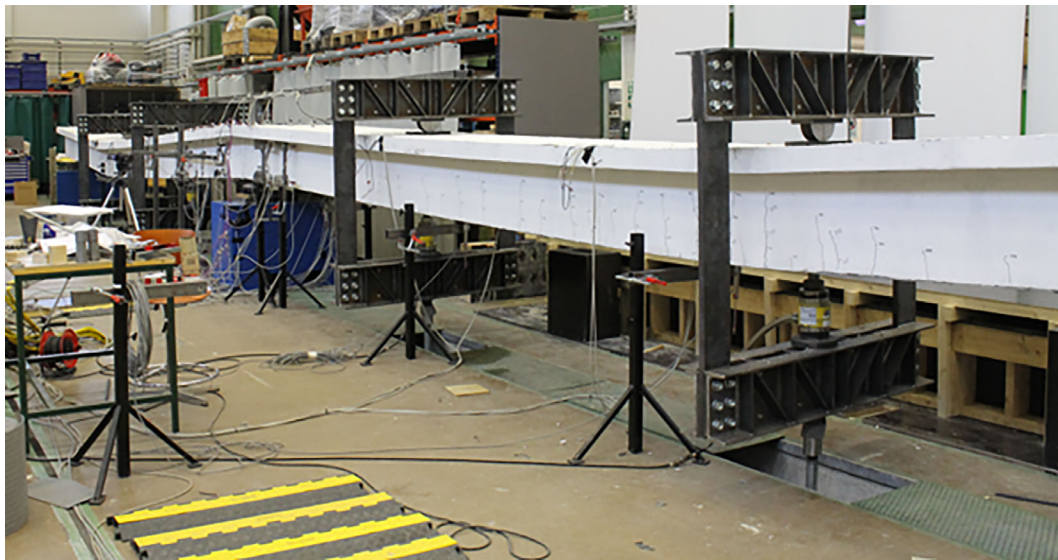


FIGURE 7 Visible plastic hinge regions in the test beam B3.

At a load level of 41% to 44% of the failure load, several new primary cracks were formed, and previously appeared cracks opened more. The crack spacing was regular, around 200 to 300 mm. When the external load was further increased, the primary cracks developed rapidly towards the compression zone and new cracks were formed until failure occurred. The width of the cracks kept increasing, particularly at the centre support areas and under the loading frames A and D, which allowed the beam to curve strongly at these areas. This indicated the yielding of the non-prestressing reinforcement. Three visible yielding regions were formed in the beams as the failure approached, as seen in Figure 7. In these three regions, the deflection and angle changes of the beam were significant. It can be assumed that the plastic capacity of the beam was reached in all three regions.

Crack formation was similar for all test beams at low load levels. When approaching the ultimate load, the distribution and direction of primary cracks differed between test beams. Crack patterns of the test beams at two load levels were drawn based on the photos taken during the load tests. First pattern is at the load level 54% to 58% of failure load and second is after failure. These are shown in Figure 8. There were less primary cracks on beam B1 with a low reinforcement ratio than in the other test beams with an intermediate reinforcement ratio. When beam B1 had reached the ultimate capacity, one wide crack and a few narrow ones were observed on the centre support area. In other beams the crack width had divided more evenly between several cracks. In beam B4, the torsion loading affected the distribution and direction of the cracks. The effect of torsion is clearly seen in the crack patterns of the test beam B4 in Figure 8.

The maximum crack width on the centre support was measured for the last time at a load level of 60% of the ultimate load for safety reasons. Crack widths were around 0.4 to 0.5 mm in all test beams except in beam B3. In B3, the maximum crack width was only 0.2 mm at the same load level. Beam B3 included compression reinforcement in the support area. That might have decreased the rotation capacity of that area and thus influenced the crack widths on the top surface.

At the first four load levels, crack formation was minimal and the measured deflections were small. When the external load was removed between the load steps, the deformations of the test beams were reverted. As the load increased, more cracks formed, and the deflections started to grow faster. After the plastic hinges on the centre support and under the loading frames A and D formed (shown in Figure 7), the deflection values grew rapidly towards failure.

When the external load was removed after the failure, the deformations of the beams were reverted and most of the cracks on the tension surface of the beam closed. This indicated that the unbonded strands had not totally yielded at the failure. In beam B4, the torsion load affected the deflection of the mid-spans in such a way that the deflection in the other span of the two-span test beam was smaller than in the other test beams loaded with bending load only.

4.2 | Results from strain gauges on reinforcement bars

At the load level 73% to 85% of the ultimate load, first visual cracks were detected on the compressive zone of

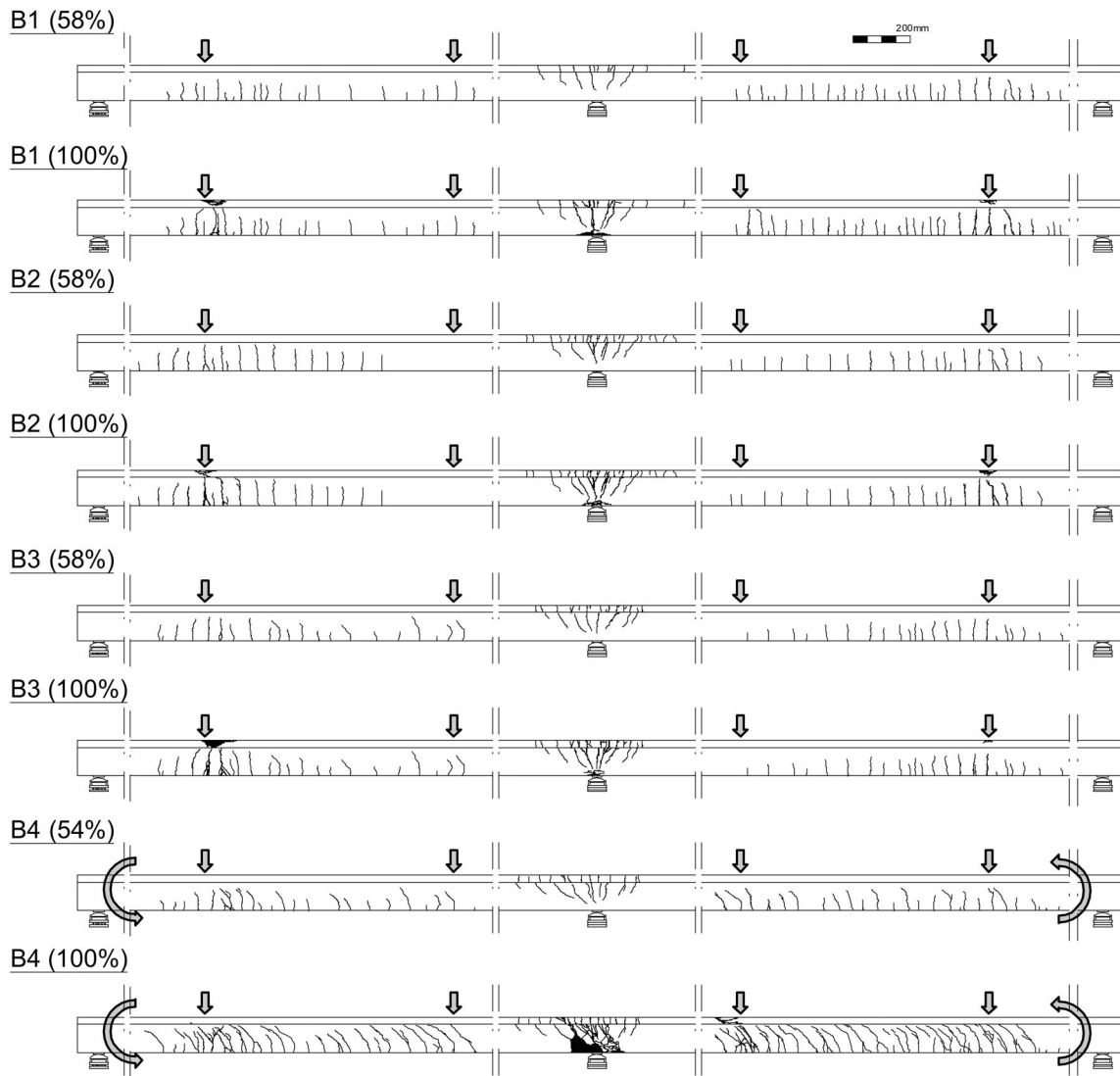


FIGURE 8 Crack patterns of the test beams.

the centre support and small concrete pieces cracked off from the concrete cover. The concrete was clearly crushed in the compression surface as the failure was approached. The failure occurred almost simultaneously in the centre support and in the mid-span.

At the support area, two electrical gauges attached to the bottom reinforcement measured the compression of the bars during the load test. When approaching the failure, the compression of the gauges in beams B1, B2, and B4 rose to the level of 6.1‰ to 7.9‰. The strains of concrete at the level of these reinforcement bars in the compression zone were clearly above the design value 3.5‰. This indicates that confinement had a significant role on the behavior of the beam at the support area. In beam B3, with compression reinforcement on the support area, the maximum compression was around 3‰. The compression reinforcement seemed to affect the maximum compression of this test beam.

Near the loading frames A and D, the strain gauges on the top reinforcement gave much lower maximum values for the compression than on the centre support. These were around 1.5‰ for all beams except for beam B4. The torsion loading affected the stresses in the spans of that beam, and the maximum measured compression was 0.5‰.

The strains of the tension reinforcement bars were also measured with strain gauges. At the failure, the reinforcement on the top of the cross-section at the centre support as well as in the bottom of the beams in the mid-spans yielded. In all test beams, the bottom reinforcement at mid-span yielded at the load level of 1100 to 1150 kN, which were 70% to 75% of the ultimate load. The maximum strains obtained from the strain gauges varied between 3.1‰ and 6.9‰. In beam B2, the strain of the bottom bars was smallest.

TABLE 3 Steel strains, curvature and rotation of the test beam at three load levels on the centre support.

Test beam	External load F_{tot} (kN)	Strain in reinforcement bar (%)		Curvature from SGB (1/m)	Rotation from LVTD (rad)	
		Compression	Tension		Total rotation	Plastic rotation
B1	890	-1.7	2.4	0.010	0.008	0.002
B1	1230	-2.3	4.1	0.015	0.026	0.020
B1	1550	-6.1	7.1	0.032	0.062	0.056
B2	890	-1.0	2.7	0.009	0.005	0.002
B2	1230	-1.6	17.3	0.045	0.018	0.015
B2	1670	-7.1	17.3	0.058	0.070	0.066
B3	907	-1.4	2.5	0.009	0.007	0.002
B3	1230	-1.9	8.6	0.025	0.020	0.015
B3	1560	-2.8	8.6	0.027	0.058	0.053
B4	910	-1.4	2.7	0.010	0.006	0.001
B4	1230	-2.2	11.0	0.031	0.028	0.023
B4	1515	-7.9	11.0	0.045	0.090	0.085

At the support, the tension reinforcement yielded at the load level of 850 to 900 kN. The largest strains measured from the strain gauges varied between 7‰ and 17‰ before the gauges were damaged. In all test beams except beam B1, the strain gauges were damaged at the final stages of the load test and did not yield reliable results after the damage. However, from the values obtained before the damage of the gauges, it can be concluded that the top reinforcement bars on the support area were clearly yielded much earlier than at the failure. The deflection of all beams during failure were high, in the range of 0.15 to 0.20 m.

4.3 | Curvature in centre support area and midspan

By using the assumptions of plane section remaining plane after bending, the curvature of a small element of length can be defined according to the concrete strain in the extreme fiber ε_c , the tension steel strain ε_s and effective height d . The curvature can be written as:

$$\varphi = \frac{\varepsilon_c + \varepsilon_s}{d} \quad (8)$$

In this study, the results from SGB on the bottom and top reinforcement bars and the distance between them in the measuring points 1, 4, and 10 were used to determine the curvature at the centre support and mid-spans. In addition, the rotation of the beam has been measured with two horizontal LVTD in points 3a, 3b, 4, and 5 as

seen in Figure 3. The curvature as well as the total rotation and the plastic rotation, which has been formed after the top reinforcement bars have yielded, have been collected in Table 3.

According to the LVTD measurement, the rotation of the centre support area was at the same magnitude in all test beams. The damage of the strain gauges (SGB) on tension reinforcement bars at the final phase of the load test influenced the determination of the curvature. The moment-curvature relationship in the centre support is shown in Figure 9 and in the mid-spans in Figure 10. In those diagrams, the moment at a particular load level were determined using the measured data of the load sensors of the bearings and the hydraulic jacks. The curvature at the same load level were determined from SGB results as explained previous paragraph. The more detailed analysis of the rotation of the centre support area would require a different measurement arrangement, such as an optical DIC measurement.

5 | EXPERIMENTAL RESULTS AND DISCUSSION

5.1 | Support reaction of test beams

The force sensors in the bearings measured the support reactions during the load test. The support reactions of the test beams were determined according to the elastic theory and measured support reactions corresponded well to each other at the low load levels before cracking.

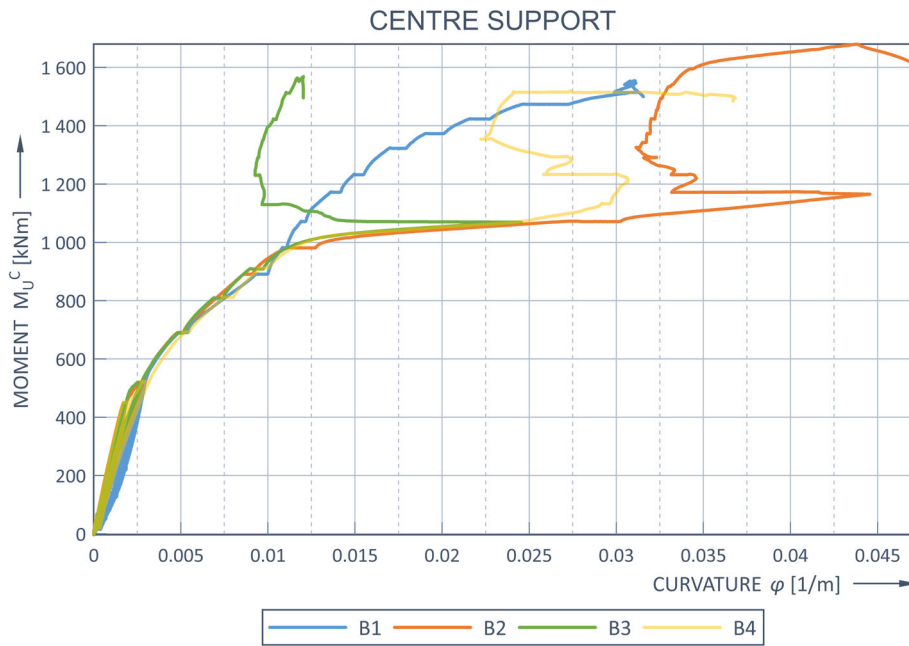


FIGURE 9 Moment-curvature relationship in the centre support.

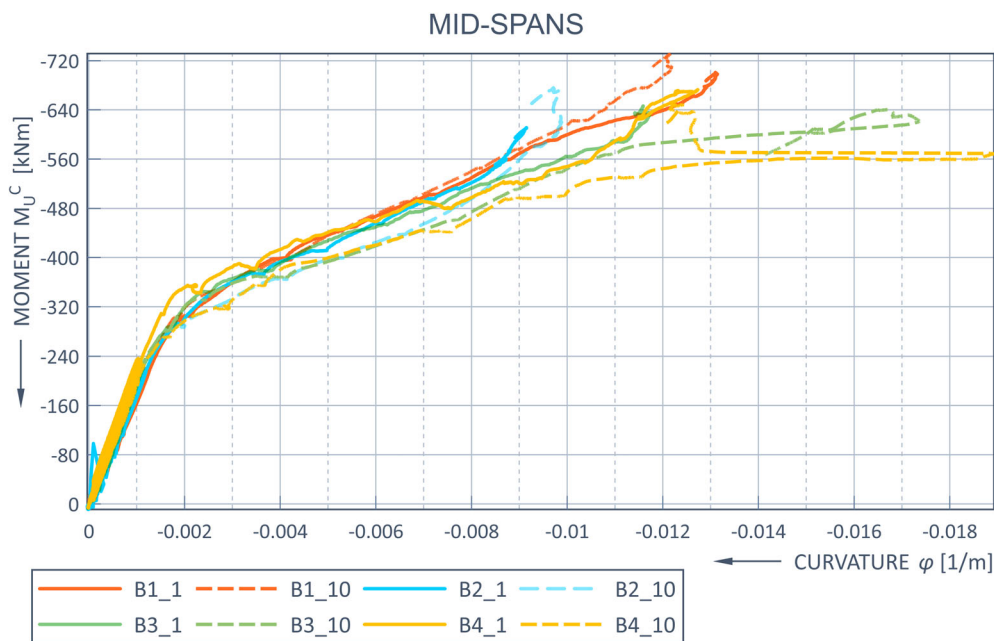


FIGURE 10 Moment-curvature relationship in the measurement points 1 and 10 (midspans).

As the external load increased, the formation of cracks increased. The value of end support reaction began to increase while the value of centre support reaction began to decrease. This indicated the redistribution of support reactions of the test beams. When the beams entered their inelastic range, measured centre support reactions corresponded better with the support reactions obtained from the nonlinear analysis as seen in Figure 11.

When approaching the failure, the end support reactions differed from the values defined with elastic theory as well as nonlinear analysis. A study of the measurement data revealed that the rotation of the beam end caused some

error to the measurement results of the force sensors in the bearings on the end supports at high loading levels. When calculating the bending moments of test beams, the measured values of the centre support were used because they were considered the most reliable.

5.2 | Comparison of tested and calculated bending moments

The bending moments in the centre support and in the locations of external loads in mid-spans can be determined

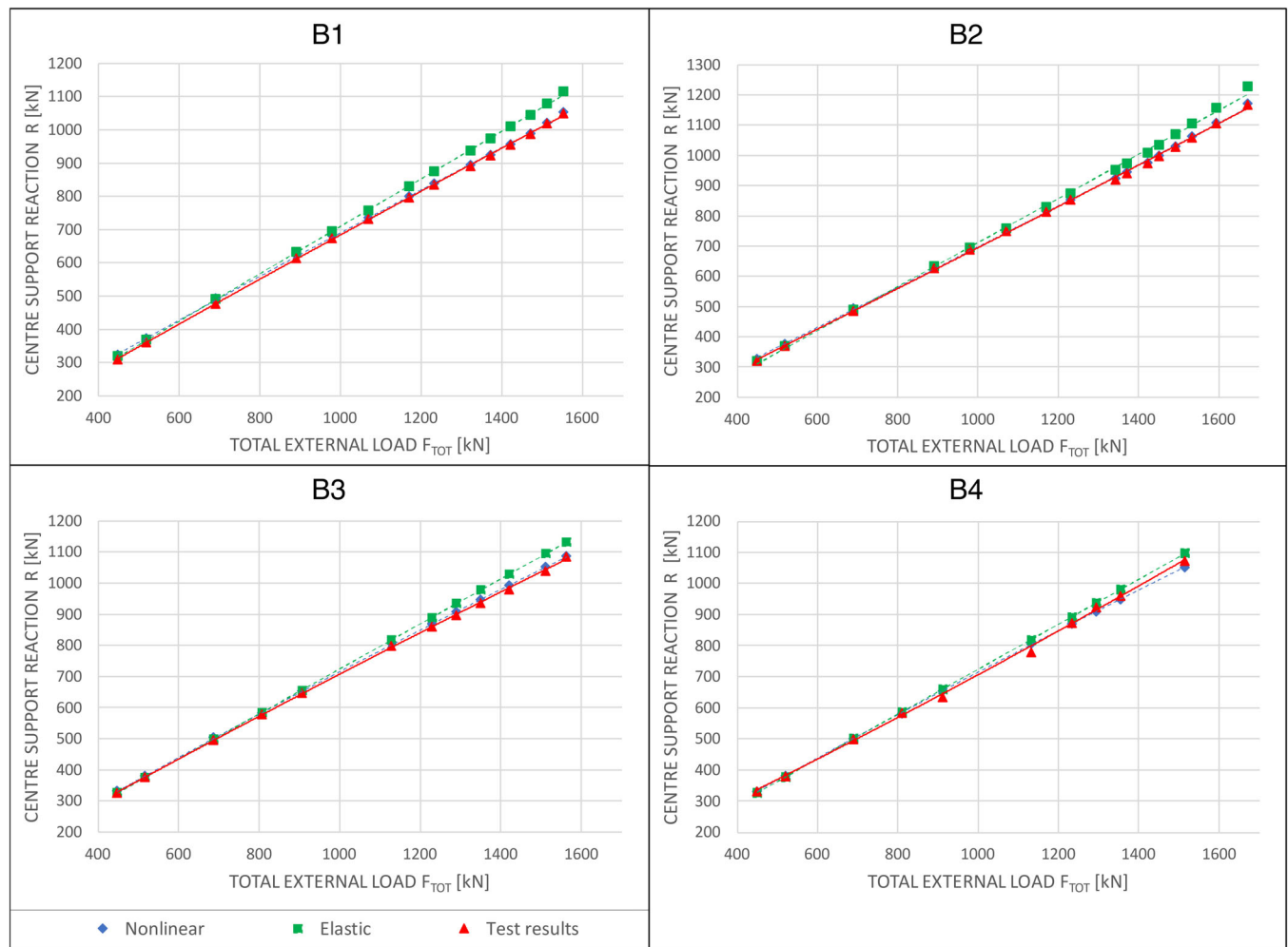


FIGURE 11 Centre support reaction.

from the measured values of support reactions and hydraulic jacks. Thus, the moment graph of the test beam can be determined during different steps of the load test. Only the values of the centre support reactions were used in the calculation as explained previously. In the comparison of tested and defined bending moments, the situation during the load test was examined because the final instrumentation had been installed only before the load test. Previously formed stresses such as self-weight of the beam and the secondary moments due to prestressing were included in the nonlinear analysis. These were around -58 kNm on the centre support and -118 kNm in the midspan. The effect of these was finally removed from the moments obtained from the nonlinear analysis so that they were comparable to the load test results. Comparison calculations were made using elastic theory and the elastic bending stiffness of the beam as well as the nonlinear analysis presented in chapter 3.¹⁴

Figure 12 shows the relationship between moment and applied load of the test beams during a load test. At the few final load steps in beams B1 and B2, the load in

the loading frames A and D was not increased so that the support area could fracture first. This can be seen in elastic moments of the mid-span in Figures 12 and 13. The results differed from the elastic trendline. In the nonlinear analysis, the stress increase in the unbonded tendons did not rise to the same level as the results obtained from the force sensor of the tendons in the test beams. The biggest differences were in beams B1 and B2. This has slightly affected the results obtained from nonlinear analysis. However, the results of the nonlinear analysis corresponded well with the test results in all test beams. The maximum moments and external load at failure have been collected in Table 4. In addition, estimated initial prestress as well as measured and calculated average stress increase in the unbonded strands are in Table 4.

The ratio of the support moment to the moment in mid-span is presented in Figure 13. Only the external load during the load test was included and self-weight and secondary moments were excluded from the assessment. The result from nonlinear analysis responds well

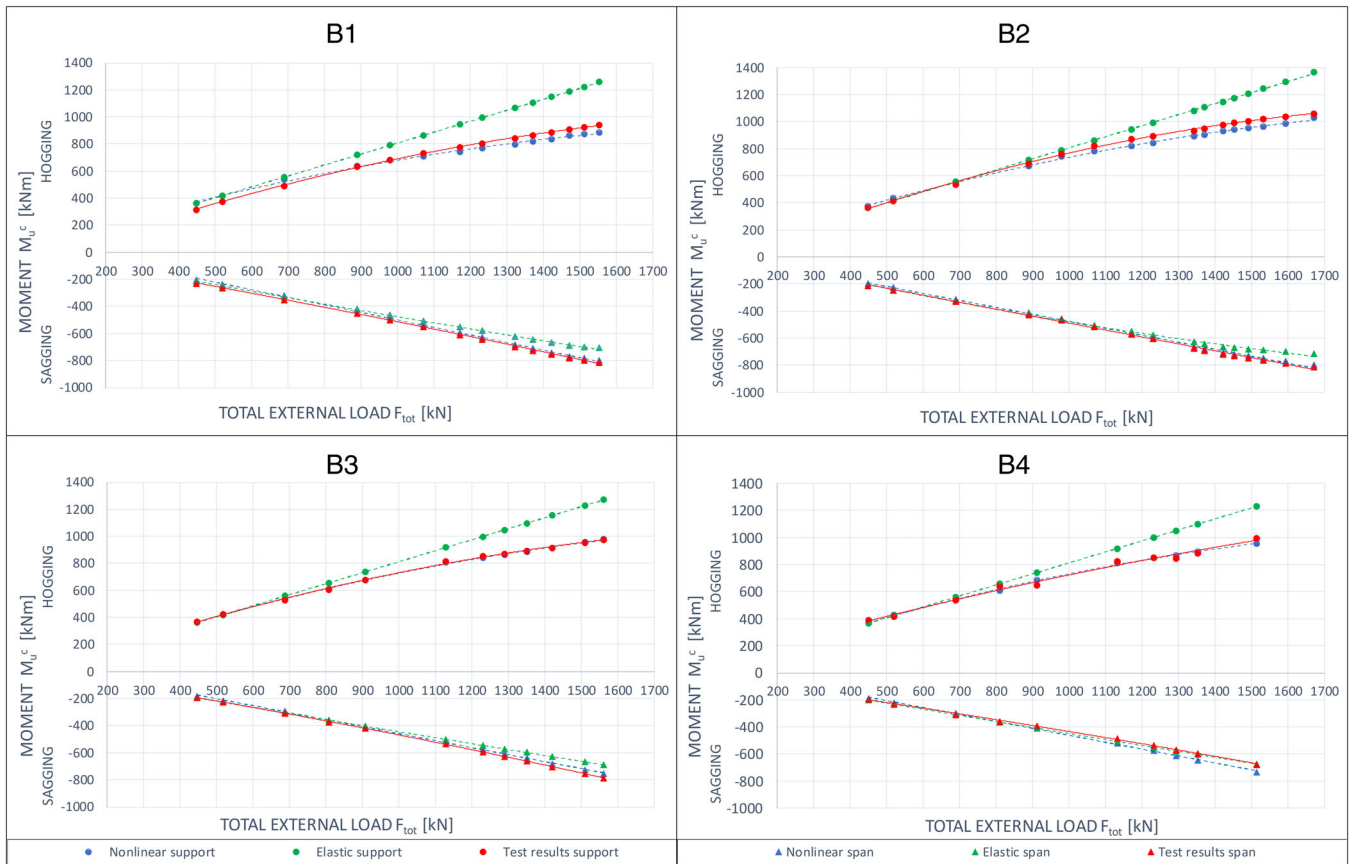


FIGURE 12 Load-moment curves of the test beams.

with the test result at the higher load levels. At low SLS load levels before cracking, the test beams behaved linearly. At these load levels, the nonlinear analysis gave distorted results because it assumes the cross-section to be fully cracked. In beam B4, the torsion loading changes the curve of the test beams. In beams B1 and B2, load ratios between the hydraulic jacks were changed at the end of the load test. This can be seen as an angle in the elastic trendline. Pang et al. presented similar behavior in their numerical assessment on unbonded prestressed concrete beams.²²

5.3 | Degree of moment redistribution

Rotation capacity is required to allow for moment redistribution. In all test beams a clear moment redistribution has been detected during the load tests. The degree of bending moment redistribution has been defined by using nonlinear analysis as well as the test results. In addition, reference values have been determined according to European standard EN 1992-1-1 and the modified ACI318 equation presented in chapter 3. The results have been collected in Table 5 with three load levels. In

Figure 14, the percentage bending moment redistribution on the centre support and the mid-span have been defined during whole load tests.

The results from nonlinear analysis were close to the values determined from the load test results. The results corresponded best to each other in beams B2 and B3. In the test beams loaded only with bending, the percentage moment redistribution on the centre support according to the test results was between 22.5% and 25.4%. All beams had the same amount of unbonded tendons, and it was significant related to the amount of ordinary bonded reinforcement. The amount of both bonded reinforcement and unbonded tendons together seems to affect the bending moment redistribution. The reinforcement index of ordinary tension steel on the support area did not seem to have notable influence on the percentage of redistribution when the amount of unbonded tendons was rather large related to the tension steel bars.

The percentages calculated according to the Eurocode were slightly higher than the values obtained from nonlinear analysis and test results. The calculations take into account the measured stress increase in the tendon at the failure.

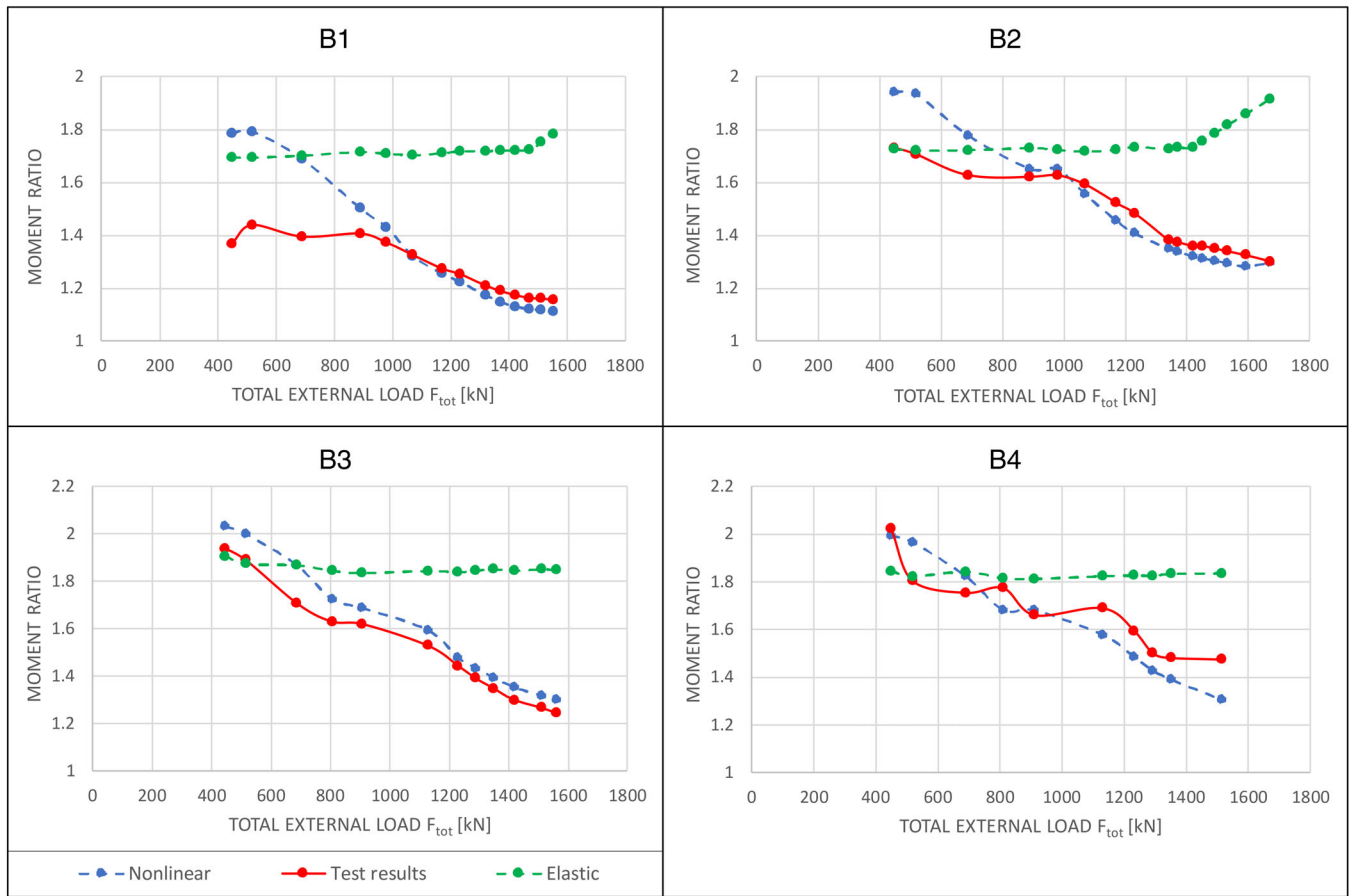


FIGURE 13 Moment ratio curves.

TABLE 4 Values of maximum moments and external loads as well as measured and calculated stress increase of tendons.

Test beam	Initial pre-stress σ_{p0} (MPa)	Max. external load F_{tot} (kN)	Test results M_u^c (kNm)		Nonlinear analysis M_u^c (kNm)		Elastic M_u^e (kNm)		Defined stress increase $\Delta\sigma_{p,ULS}$ (MPa)	Measured stress increase $\Delta\sigma_{p,ULS}$ (MPa)
			Support	Mid-span	Support	Mid-span	Support	Mid-span		
B1	1040	1553	940	-813	889	-800	1259	-707	512	655
B2	940	1671	1059	-815	1029	-795	1366	-714	647	775
B3	990	1562	977	-786	981	-755	1271	-689	476	687
B4	965	1515	997	-677	957	-734	1233	-672	458	638

When using the proposed modification of the ACI318 equation, the maximum value for steel strain obtained from load test was used. The results from the equation were massive when the steel strain increased to the maximum. The proposed equation for ACI318 has an empirical nature. The problem with empirical formulas is that we do not know whether the assumptions of the equation work in this context. In this context, the formula yielded overestimated values for moment redistribution.

In the mid-span, the bending moment capacity of the test beams was similar in all test beams. During the load test, the redistributed moment in the mid-span was 14% to 15% in beams B1 to B3. In beam B4, the torsion loading changed the behavior of the mid-span so that the moment decreased in the other span due to torsion. The torsion load was added and removed at intervals during the load test. This can be seen as a deviation of the trendline of beam B4. According to nonlinear analysis,

TABLE 5 Percentage bending moment redistribution on the centre support at three load levels.

Test beam	External load F_{tot} (kN)	Mechanical reinforcement ratio ω_s	Test results M_u^c (kNm)	Nonlinear analysis M_u^c (kNm)	Elastic M_u^c (kNm)	δ (%)			
						Load test	Nonlinear analysis	Proposed equation ACI318	EN 1992-1-1
B1	890	0.0229	631	639	719	12.2	11.1	6.7	
B1	1230	0.0229	804	770	995	19.2	22.7	11.4	
B1	1550	0.0229	940	889	1259	25.4	29.4	19.7	28.6
B2	890	0.0415	689	676	719	4.2	6.0	15.6	
B2	1230	0.0415	897	842	994	9.8	15.4	99.7	
B2	1670	0.0415	1059	1029	1366	22.5	24.6	99.7	26.8
B3	907	0.0470	680	679	738	7.8	8.0	14.1	
B3	1230	0.0470	853	844	1000	14.7	15.6	48.4	
B3	1560	0.0470	977	981	1271	23.1	22.8	48.4	28.1
B4	910	0.0458	647	686	742	12.8	7.5	15.4	
B4	1230	0.0458	853	852	1003	14.9	15.0	62.6	
B4	1515	0.0458	997	957	1233	19.1	22.4	62.6	25.5

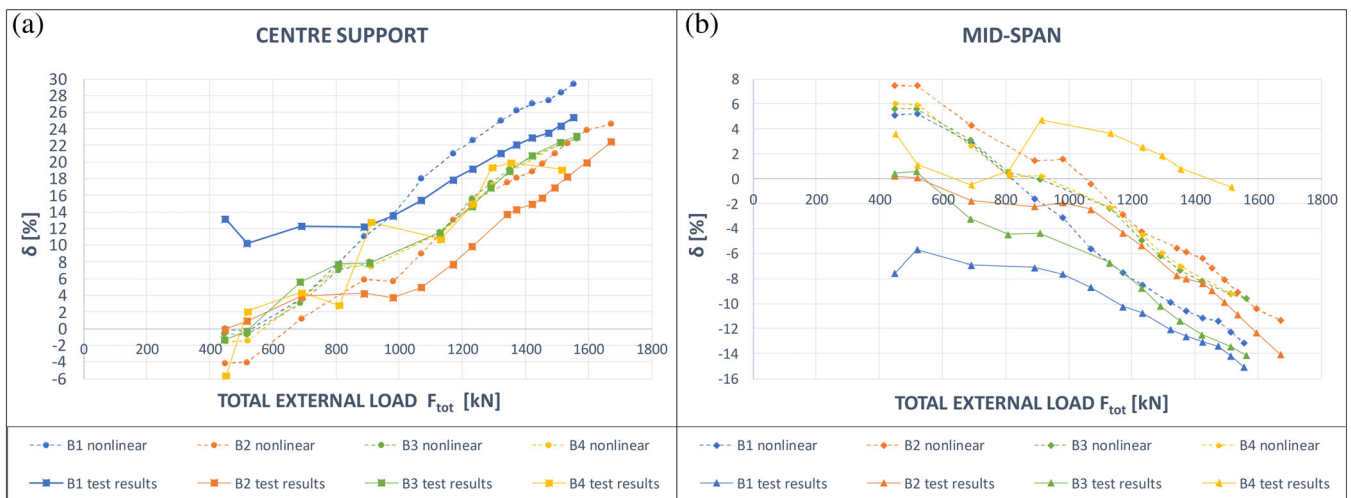


FIGURE 14 Degree of moment redistribution on centre support (a) and in mid-span (b).

the moment redistribution in the mid-span was slightly smaller, around 9.2% to 13.1%.

The test results of the centre support area show two changing points in the graphs in Figure 14: the first at the load level of 700 kN when the crack formation stabilized and the second at the load level of 900 to 950 kN when the non-prestressed reinforcement yielded in the tension fiber. Similar points can also be observed in the graphs of the mid-span. The moments started to clearly transfer from support to the spans after the non-prestressed reinforcement had yielded in both centre support and mid-spans. In the ordinary reinforced

concrete beam, the moment redistribution normally starts earlier.

6 | CONCLUSION

Four continuous two-span concrete beams prestressed with unbonded tendons were fabricated and loaded up to failure at the laboratory of Civil Engineering in Tampere University. All test beams were loaded by bending, but one test beam had torsion load in addition to bending. The following are conclusions derived from the load test results:

1. Moment redistribution clearly occurred on all test beams.
2. The amount of both bonded and unbonded reinforcement together seems to affect the bending moment redistribution of the centre support area in the two-span beam.
3. Moments started to transfer from support to the spans after the non-prestressed reinforcement had yielded in both centre support and mid-spans. The test beams achieved a deflection of $L/50$. If such a beam is part of a structural system post-tensioned with unbonded tendons, for example, floor structure, the whole system has a high deformability.
4. Percentage moment redistribution obtained from test results corresponded well with the results from nonlinear analysis and quite well with the results defined by equations from the European standard.
5. The results from nonlinear analysis corresponded best with the test results in beam B3. For this beam, the concrete material model used in the analysis matched well with the concrete compression results obtained from the load test. The material model used in nonlinear analysis has an essential effect on the results obtained from the analysis.
6. Based on the test results, the torsion loading did not substantially weaken the ability of the moment redistribution of the test beam.

ACKNOWLEDGMENTS

The authors gratefully acknowledge the financial support provided by the Finnish Concrete Industry. The authors would also like to thank Mr. Tomi Strander, Mr. Lauri Kuusela, Mr. Markus Hakala and Mr. Mika Vuorela for their assistance in the laboratory phase of this study.

DATA AVAILABILITY STATEMENT

Data available on request from the authors.


ORCID

Tarja Nakari  <https://orcid.org/0000-0003-1112-9531>

Joonas Tulonen  <https://orcid.org/0000-0002-0879-244X>

Olli Asp  <https://orcid.org/0000-0003-4022-8336>

Ulla Kytölä  <https://orcid.org/0000-0003-0645-8146>

Anssi Laaksonen  <https://orcid.org/0000-0001-8459-7470>

REFERENCES

1. Mattock AH, Yamazaki J, Kattula BT. Comparative study of Prestressed concrete beams, with and without bond. *ACI J*. 1971;68(2):116–25.
2. Harajli MH. On the stress in unbonded tendons at ultimate: critical assessment and proposed changes. *ACI Struct J*. 2006; 103(6):803–12.
3. Harajli MH. Proposed modification of AASHTO-LRFD for computing stress in Unbonded tendons at ultimate. *J Bridge Eng ASCE*. 2011;16(6):828–38.
4. Harajli MH. Tendon stress at ultimate in continuous Unbonded post-tensioned members: proposed modification of ACI 318, Eq. (18-4) and (18-5). *ACI Struct J*. 2012;109(2): 183–92.
5. Naaman AE, Alkhairi FM. Stress at ultimate in unbonded post-tensioned tendons: part 2—proposed methodology. *ACI Struct J*. 1991;88(6):683–92.
6. Kordina K, Hegger J. Zur Ermittlung der Biegebruch-Tragfähigkeit bei Vorspannung ohne Verbund. *Beton- Und Stahlbetonbau*. 1987;Heft 4:85–90.
7. Zhou W, Zheng WZ. Experimental research on plastic design method and moment redistribution in continuous beams Prestressed with Unbonded tendons. *Mag Concr Res*. 2010;62(1): 51–64.
8. Mossor K. Differences in moment redistribution in concrete beams prestressed with bonded and unbonded tendons. *PCI J*. 2022;67:12.
9. Weller B. Experimentelle Untersuchungen zum Biegetragverhalten von Durchlaufträgern mit Vorspannung ohne Verbund. *Deutscher Ausschuss für Stahlbeton*. 1988;391:73–125.
10. Maguire M, Collins WN, Halbe KR, Roberts-Wollmann CL. Multi-span members with unbonded tendons: ultimate strength behavior. *ACI Struct J*. 2016;113(S18):195–204.
11. Pujol S, Fick DR, Fargier-Gabaldón LB. Test of 90-foot post-tensioned concrete girder with Unbonded tendons. *ACI Struct J*. 2021;118(S96):115–22.
12. Kim SK, Lee DH. Nonlinear analysis method for continuous post-tensioned concrete members with Unbonded tendons. *Eng Struct*. 2012;40:487–500.
13. Vu NA, Castel A, François R. Response of post-tensioned concrete beams with unbonded tendons including serviceability and ultimate state. *Eng Struct*. 2010;32(2):556–9.
14. Nakari T, Laaksonen A. Determination of the stress increase of the Unbonded tendon in a continuous concrete beam at ultimate capacity using nonlinear analysis. *Nordic Concr Res*. 2021;64:109–28.
15. Lou T, Peng C, Min D, Sun W. Moment redistribution in Unbonded Prestressed concrete members: proposed modification of ACI equation. *ACI Struct J*. 2020;117(S125):71–80.
16. European Standard EN 1992-1-1. Eurocode 2: Design of concrete structures—Part 1-1: General rules and rules for buildings. 2005 226 pp.
17. Test certificate for seven-wire strand, TYCSA PSC. 2020.
18. European Standard EN 1991-1-1. Eurocode 1, Actions on structures. Part 1-1: General actions. Densities, self-weight, imposed loads for building, 2002, 44 pp.
19. European standard EN. Eurocode: Basis of Structural Design, 2002, 120 pp. 1990.
20. LUSAS. Academic bridge plus software.
21. ACI Committee 318. Building code requirements for structural concrete (ACI 318-14) and commentary (ACI 318R-14). Farmington Hills, MI: American Concrete Institute; 2014. p. 519.
22. Pang M, Liu X, Dong Y, Lou T. Numerical assessment on bonded and Unbonded Prestressed concrete beams. *Buildings*. 2022;12(1658):16.

AUTHOR BIOGRAPHIES



Tarja Nakari, Ph.D. Student, Faculty of Built Environment—Concrete and Bridge Structures, Tampere University, Tampere, Finland.



Joonas Tulonen, Ph.D. Student, Faculty of Built Environment—Concrete and Bridge Structures, Tampere University, Tampere, Finland.



Olli Asp, Ph.D. Student, Faculty of Built Environment—Concrete and Bridge Structures, Tampere University, Tampere, Finland.



Ulla Kytölä, Ph.D. Student, Faculty of Built Environment—Concrete and Bridge Structures, Tampere University, Tampere, Finland.



Anssi Laaksonen, Professor, Faculty of Built Environment—Concrete and Bridge Structures, Tampere University, Tampere, Finland.

How to cite this article: Nakari T, Tulonen J, Asp O, Kytölä U, Laaksonen A. Experimental study of moment redistribution in continuous concrete beams prestressed with unbonded tendons. *Structural Concrete*. 2024. <https://doi.org/10.1002/suco.202300793>